

Controlled Electron-Induced Fabrication of Metallic Nanostructures on 1 nm Thick Membranes

Christian Preischl, Linh Hoang Le, Elif Bilgilişoy, Florian Vollnhals, Armin Götzhäuser, and Hubertus Marbach*

Functional hybrids comprising metallic nanostructures connected and protected by nonmetallic 2D materials are envisioned as miniaturized components for applications in optics, electronics, and magnetics. A promising strategy to build such elements is the direct writing of metallic nanostructures by focused electron beam induced processing (FEBIP) onto insulating 2D materials. Carbon nanomembranes (CNMs), produced via electron-induced crosslinking of self-assembled monolayers (SAMs), are ultrathin and flexible films; their thickness as well as their mechanical and electrical properties are determined by the specific choice of self-assembling molecules. In this work, functionalized CNMs are produced via electron beam induced deposition of $\text{Fe}(\text{CO})_5$ onto terphenylthiol SAMs. Clean iron nanostructures of arbitrary size and shape are deposited on the SAMs, and the SAMs are then crosslinked into CNMs. The functionalized CNMs are then transferred onto either solid substrates or onto grids to obtain freestanding metal/CNM hybrid structures. Iron nanostructures with predefined shapes on top of 1 nm thin freestanding CNMs are realized; they stay intact during the fabrication procedures and remain mechanically stable. Combining the ease and versatility of SAMs with the flexibility of FEBIP thus leads to a route for the fabrication of functional hybrid nanostructures.


electron-induced crosslinking of aromatic self-assembled monolayers (SAMs).^[6] This process results in the formation of carbon nanomembranes (CNM), which are 2D materials with very versatile properties^[7] such as very high thermal^[8] and mechanical^[9] stability and tunable electrical conductivity and stiffness.^[10] The thickness, surface termination, porosity, etc., of CNMs can be tailored by the choice of the molecules forming the SAM.^[11] Furthermore, the CNM can be transferred onto arbitrary substrates or onto porous structures and grids to obtain freestanding 2D membranes.^[12] It was shown that CNM multilayers and 2D heterostructures can be produced by mechanical stacking of CNMs, graphene, and MoS_2 sheets,^[13] and stacks of CNMs and graphene were used to build all-carbon capacitors.^[14] CNMs with sub-nm pores have been fabricated and used to separate ions from water during osmosis.^[15] Freestanding CNMs were further used as mechanically stable and nonconductive supports for microm-

eter-scale metallic patterns.^[16] The resulting almost freestanding conductive structures open up new possibilities to design plasmonic and photonic devices and nanoelectromechanical systems (NEMS).^[17] In case of ferromagnetic freestanding structures, one may even think about switching properties, for example, the permeability of the CNMs by applying an external magnetic field. So far, micrometer-scale conductive structures were mostly fabricated on CNMs by using classical resist based electron beam lithography.^[16] It was shown that nanometer thin gold deposits on top of a freestanding CNM can be used as plasmonic nanoresonators.^[18] This might open up the possibility for the fabrication of ultrathin optical devices. In the present study, we expand on this topic by exploring resistless focused electron beam induced processing (FEBIP) to create metallic nanostructures on freestanding and nonconductive CNMs.

FEBIP utilizes a focused electron beam to directly create nanostructures by a controlled reaction with volatile precursor molecules. Specifically, we apply electron beam induced deposition (EBID).^[19] In EBID, precursor molecules, which are usually metal-organic compounds, are decomposed by the impact of the electron beam such that the nonvolatile metal center forms a deposit, whereas the volatile organic fragments desorb. Compared to other lithographic tools, EBID exhibits the capability to

C. Preischl, E. Bilgilişoy, Dr. F. Vollnhals, Dr. H. Marbach
Physikalische Chemie II
Friedrich-Alexander Universität Erlangen-Nürnberg
Erlangen 91058, Germany
E-mail: hubertus.marbach@fau.de

L. H. Le, Prof. A. Götzhäuser
Fakultät für Physik
Universität Bielefeld
Bielefeld 33615, Germany

 The ORCID identification number(s) for the author(s) of this article can be found under <https://doi.org/10.1002/smll.202003947>.

© 2020 The Authors. Published by Wiley-VCH GmbH. This is an open access article under the terms of the Creative Commons Attribution License, which permits use, distribution and reproduction in any medium, provided the original work is properly cited.

DOI: 10.1002/smll.202003947

directly produce nanostructures of arbitrary shape and size^[20] and the deposited material can be varied with the huge amount of available precursors.^[19b] EBID experiments on thin membranes are reported in literature to some extent.^[21] In these studies, the focus is on the role of secondary electrons, which are reduced in number compared to bulk substrates and thus smaller deposits from EBID are possible. In addition, either multilayer CNMs were used^[21b] or the EBID experiments were conducted with a scanning transmission electron microscope (STEM) using high electron energies and low current aiming for ultrahigh resolution EBID.^[21] It was also reported that on very thin membranes the growth rate is not constant.^[21b]

Apparently, the fabrication of well-defined nanostructures by EBID is challenging on freestanding ultrathin 2D materials; we therefore explored a novel fabrication route sketched in **Figure 1**. In our approach, we thus start with an EBID nanopatterning step on a bulk substrate, i.e., a SAM of terphenylthiol (TPT) on a gold substrate (cf. Figure 1a,b) that facilitates the deposition of well-defined iron nanostructures via the decomposition of $\text{Fe}(\text{CO})_5$ molecules. During EBID the SAM located in the area below the resulting deposit is simultaneously crosslinked into a CNM (indicated by the red square shown in Figure 1a). The fabrication of the iron nanostructures is thus performed *before* the SAM is crosslinked. This avoids the known charging problems^[22] that would be present during the deposition onto some nonconductive-type freestanding CNMs. In addition, freestanding 1 nm-thick CNMs may rupture upon a prolonged impact of a highly focused electron beam. An example is documented in Figure S1 (Supporting information) with a CNM from 4'-amino-1,1'-biphenyl-4-thiol (NBPT) with a thickness of ≈ 1 nm. Generally, the deposited nanostructures exhibit very high Fe purity (90 at% Fe) (cf. Figure S2, Supporting

Information), as was also reported in previous studies under ultrahigh vacuum (UHV) conditions. In particular, autocatalytic growth (AG) processes, which proceeds after the electron irradiation step, yielded iron structures with a purity larger than 95%.^[23] Figure S2 (Supporting Information) also reveals that no iron is deposited in close proximity to the irradiated areas. In the next step, the aromatic SAM is transformed into a 2D CNM by low-energy electron-induced crosslinking as illustrated in Figure 1c. The transfer of the CNM is realized by spincoating the sample with poly(methyl methacrylate) (PMMA) and subsequent etching of the Au layer in a solution of $\text{KI}/\text{I}_2/\text{H}_2\text{O}$. In this critical etching step, the deposited iron nanostructures are sandwiched between PMMA and the CNM, which protects their chemical and structural integrity and prevents them from mechanical forces (see Figure 1d). The PMMA/Fe/CNM hybrid can then be transferred to any substrate. In our approach, we transferred it either onto a TEM grid or onto a SiO_2 sample as illustrated in Figure 1e,f. Finally, the PMMA is removed by dissolution in acetone while the Fe nanostructure remains on the CNM. In Figure 1g the actual relation of the thickness of the CNM to the dimension of the aerial iron deposits (cf. the deposit shown in Figure 3e) is illustrated. While the high mechanical stability of the CNM was documented before,^[9] it needs to be explored if the metallic EBID structures can be transferred intact with the membrane. The second important aspect is to investigate if and how the nanostructures might be modified due to the exposure to $\text{KI}/\text{I}_2/\text{H}_2\text{O}$ and ambient conditions. With this method nanofunctionalized 2D materials can be fabricated. Compared to other approaches, like the direct etching of graphene,^[24] where the 2D material is removed on the nanometer scale, our concept allows producing metallic nanostructures of arbitrary shape, e.g., circles, on top

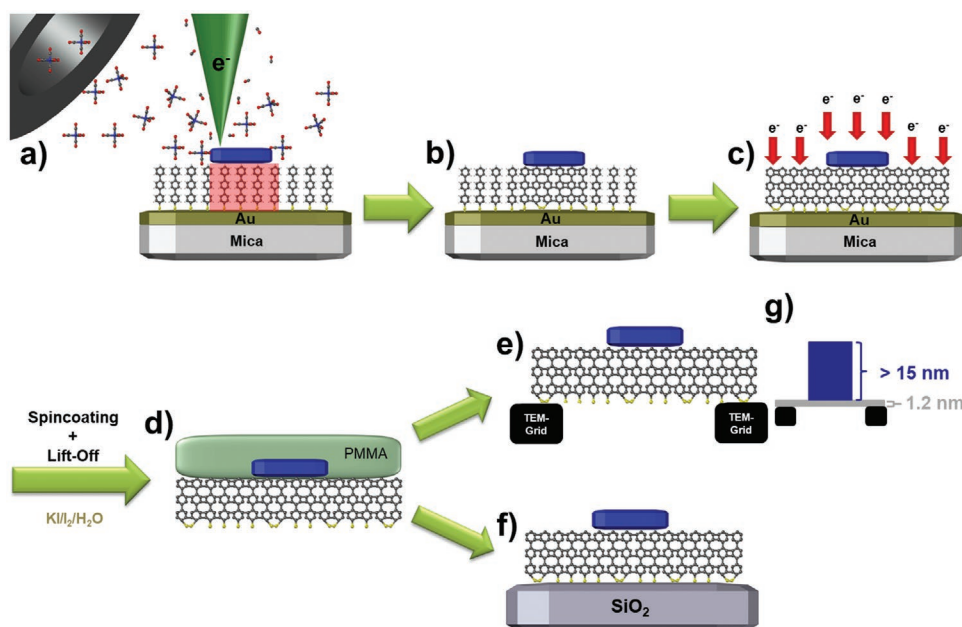


Figure 1. Scheme of the fabrication process: a) EBID of $\text{Fe}(\text{CO})_5$ onto a TPT SAM on Au/mica; the blue feature is the resulting Fe EBID deposit; the red square indicates that during EBID simultaneously the irradiated area of the SAM is crosslinked; b) Fe nanostructure on TPT SAM; the area below the nanostructure is already transformed into a CNM; c) crosslinking of aromatic SAM with low energy electrons (≈ 50 eV) via flood gun; d) sample is spin-coated with PMMA and removed from the substrate by etching the Au layer with $\text{KI}/\text{I}_2/\text{H}_2\text{O}$; e, f) membrane is transferred onto TEM grid or onto SiO_2 , PMMA is removed by acetone; g) real dimensions of a typical aerial Fe deposit on top of a CNM.

of a freestanding 2D material. This aspect increases the potential for future applications, also in regard to the ferromagnetic properties of our iron deposits.^[25]

Figure 2 depicts SEM images of Fe EBID structures before and after the formation of the CNM and subsequent transfers onto a TEM grid (left column) and onto a bulk SiO₂ substrate (right column) along with the corresponding sketches. The pattern we have created for the iron nanostructures resembles the schematic of crosslinked TPT SAMs, cf. Figure 1c. In Figure 2a,b, two patterns are shown as they were deposited on the SAM/Au at electron doses of 1.86 and 2.07 C cm⁻², respectively. After the transfer steps, the structures remain intact. Figure 2c,d depicts Fe nanostructures after transfer onto a TEM grid/400 mesh (Figure 2c) and SiO₂ (Figure 2d), respectively.

Comparing the structured iron deposits before and after crosslinking plus the subsequent transfer, it becomes obvious that these stay intact and retain their original shape during the procedure without major modifications. Thus, the metallic EBID deposit could be transferred successfully, leading to iron nanostructures on top of a freestanding 1.2 nm thin organic membrane as well as on a SiO₂ bulk substrate. There are some smaller ruptures in the freestanding membrane, which are most probably caused by particles located on the SAM already before the writing process (see Figure 2a,c). The two larger ruptures are exactly on the position where the two particles were located before the transfer. This result conclusively demonstrates the flexibility of the fabrication method, as the PMMA/CNM hybrid with the embedded EBID nanostructures can be transferred in principle to any substrate of choice. Consequently, the fabrication method bears very high potential for applications in nanoelectronics, especially regarding the demonstrated high conductivity of EBID iron structures fabricated in UHV.^[26] Another promising feature are the ferromagnetic properties of the deposited iron structures^[25] which might open up possibilities to fabricate 3D configurations at the nanoscale via folding of 2D structures.^[27] Previous TEM studies about iron nanostructures fabricated in UHV with EBID followed by autocatalytic growth demonstrate that the resulting nanostructures consist of α -Fe and Fe₃O₄.^[28] In Figure S3a,b (Supporting Information), the high flexibility and foldability of the CNM even with iron nanostructure on top is shown. The corresponding high-resolution image and intensity line profile for the nanostructure shown are depicted in Figure 2e,f. The width of the lines shown in Figure 2 is between 60 and 75 nm, whereas the height determined by atomic force microscopy (AFM) is between 2 and 4 nm (see Figure 2g,h). We propose that the fabrication method described in the work at hand is capable to create even smaller structures, since it was shown that thin organic layers (like a SAM) can effectively reduce electron proximity effects and thus the lateral size of deposits in EBID.^[29]

In **Figure 3a**, a SEM image of a different Fe nanostructure on a CNM is depicted after the transfer process. After inspection of the corresponding blow-up image (Figure 3b), it becomes evident that the iron nanowires are fully intact after transfer. However, small ruptures in the membrane are visible, most likely, these were produced during acquisition of the high-magnification image. The fact that the CNM membrane tends to rupture under electron exposure might open up new

possibilities by itself, like the fabrication of completely free-standing iron nanostructures. We also observe that imperfections visible in SEM after crosslinking, i.e., before the transfer, are likely to trigger ruptures of the membrane (cf. Figure 2a,c). Local Auger electron spectroscopy (AES) (Figure 3i, green spectrum) evidences that a high amount of iron is present in the nanostructure. The nanostructure contains oxygen, which can be explained by the exposure to ambient during the transfer. In addition, scanning Auger microscopy was performed, depicted in Figure 3c. From this spectromicroscopic image it is evident that the whole nanostructure contains significant amounts of iron.

In order to acquire conclusive spectroscopic information and to explore more expanded shapes, larger structures with a size of several micrometers (consisting of a rectangle and arrow below) were fabricated on TPT (Au(111)/mica) with Fe(CO)₅ via EBID + AG. The SEM image of one of these structures is depicted in Figure 3d. In Figure 3e, the SEM image of this larger iron nanostructure is shown after crosslinking and transfer to a SiO₂ substrate. While the deposit still in UHV contains mainly iron (cf. Figure S2, Supporting Information) the local Auger electron spectrum (Figure 3i, dark red spectrum) of the structure after the transfer evidences that the structure is oxidized during the transfer and a significant carbon content is also observed. The latter most likely originates from residual PMMA that was not removed with acetone. This image is consistent with the fact that 5 min of Ar sputtering (bright red spectra in Figure 3i) is sufficient to remove the carbon and to obtain iron oxide with a very high purity (84 at% Fe). In Figure 3f, a zoom-in SEM image of the transferred structure depicted in Figure 3e is depicted. One observes the typical cubic iron crystals characteristic for deposition due to autocatalytic growth.^[23] These cubic crystals are maintained through the transfer process and exhibit a height of roughly 10 to 20 nm as estimated by AFM (cf. Figure 3g,h), i.e., ≈ 10 – 20 times thicker than the actual membrane. Thus, the membrane is stable enough to transfer comparably large nanostructures without major alterations of the latter. From these results, we can conclude that not only the shape of the nanostructures is robust to the transfer but also the chemical composition remains besides moderate oxidation due to exposure to ambient. This is especially important for the targeted functionality of the latter since it was reported that even oxidized Fe-EBID structures maintain high conductivity^[26] and their ferromagnetic properties.^[25,30] This again demonstrates the potential for application in nanoelectronics.

In summary, we present a novel and powerful method to fabricate metallic nanostructures on ultrathin organic 2D materials. The ultrathin membranes with precisely defined iron nanostructures on top can practically be transferred to any bulk substrate, or onto a grid to obtain a freestanding, nanostructured membrane. We conclusively demonstrated that the deposited nanostructures maintain their shape and with few restrictions their chemical composition during the transfer process, i.e., the treatment in KI/I₂/H₂O solution had no detectable influence. To overcome the oxidation upon exposure to ambient one might use a protective capping layer as reported previously.^[30] By stacking the nanostructured CNMs, one might target the fabrication of layered complex electronic

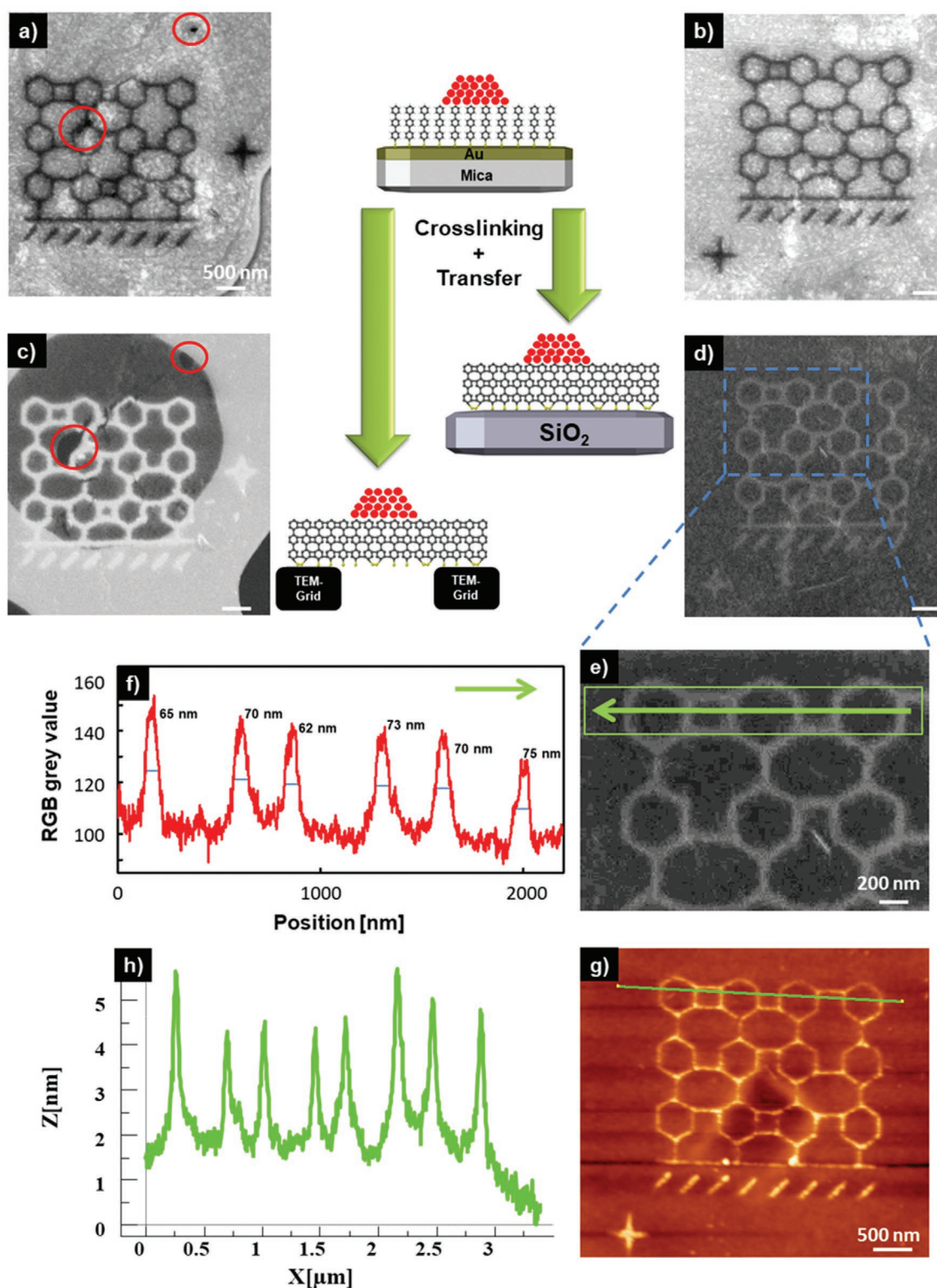


Figure 2. Schematic drawing of the transfer process and the corresponding SEM images of a) EBID nanostructure on SAM on Au(111)/mica fabricated with the precursor $\text{Fe}(\text{CO})_5$ (beam parameters: 15 kV, 400 pA, electron dose: 1.86 C cm^{-2} , AG time: 1 h); b) EBID nanostructure on SAM on Au(111)/mica fabricated with the precursor $\text{Fe}(\text{CO})_5$ (beam parameters: 15 kV, 400 pA, electron dose: 2.07 C cm^{-2} , AG time: 1 h 27 min); c) the nanostructure depicted in (a) after transfer onto TEM grid; the red circles indicate positions of particles/defects before the transfer, which obviously lead to ruptures in the freestanding CNM; d) the nanostructure depicted in (b) after transfer process onto SiO₂; e) blow-up of the corresponding nanostructure; f) integrated intensity line profile with correspondingly estimated full width at half maximum values extracted from the high-magnification SEM image shown in (e). g) AFM image of the CNM Fe nanostructure which was transferred on SiO₂; h) height profile of the structure from (g).

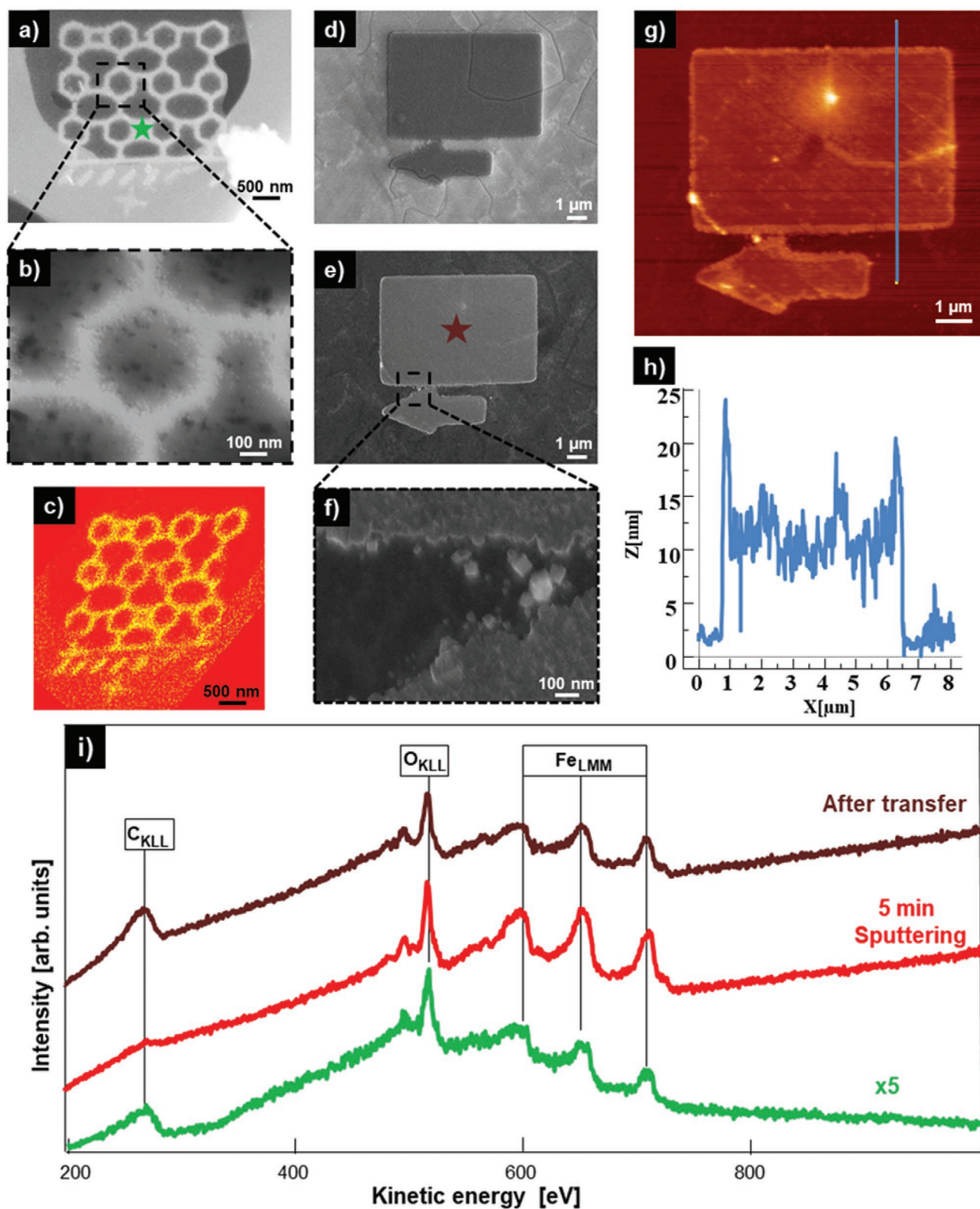


Figure 3. a) Freestanding TPT membrane with Fe nanostructure after transfer on TEM grid; b) blow-up of the freestanding Fe nanostructure; c) scanning Auger microscopy image of the freestanding Fe nanostructure (Fe LMM peak 703 eV minus background at 735 eV); d) SEM image of a large Fe marker structure fabricated with EBID on SAM TPT on Au(111)/mica (beam parameters: 15 kV, 400 pA, electron dose: 0.93 C cm⁻², AG time: 8 h 46 min); e) SEM image of the large Fe marker structure depicted in (d) after the transfer to bulk SiO₂; f) SEM zoom-in of detail in (e); g) AFM image of the CNM Fe nanostructure shown in (e); h) height profile of the structure from (g); i) local AE spectra recorded at the positions indicated with, respectively, colored stars.

structures, in which the CNMs are anticipated to act as ≈ 1 nm-thin insulating layer between the conductive nanostructures. With the plethora of available precursors in FEBIP, there are almost infinite possibilities to target nanostructuring with other materials than Fe. Recent studies show that Ag nanostructures with a purity of 76 at% can be fabricated via EBID.^[31] Combining EBID with a simultaneous cleaning upon water dosage even highly pure Au (91 at%) nanostructures can be produced.^[32] The combination of the versatile properties of the CNMs with the flexibility in producing arbitrary shaped metallic nanostructures in FEBIP opens up completely new ways for optical, electrical, magnetic, and nanomechanical applications.

Experimental Section

The precursors NBPT (Taros Chemicals GmbH & Co.KG, 97%) and TPT (Sigma-Aldrich, 97%) were sublimated before use. Au (111)/mica substrates (Georg Albert PVD) employed in this study comprise a 300 nm-thick Au layer on mica. The substrates were exposed to UV-ozone cleaner (UVOH 150 LAB FHR) for 3 min prior to immersion for 20 min and rinsing in ethanol (VWR BHD Chemicals, 99.9%). SAMs on the gold substrates can be achieved as the procedures described elsewhere.^[9,12] Briefly, the gold wafers were soaked in an ≈ 10 mmol solution of a precursor and degassed N,N-dimethylformamide (DMF, Sigma-Aldrich, 99.8%) in argon atmosphere for a period of time (72 h at room temperature for NBPT and 24 h at 70 °C for TPT). Thorough rinsing in DMF and subsequently in ethanol, followed by a stream of nitrogen for drying, resulted in SAMs, which are involved in further EBID experiments.

In order to transfer CNMs onto tertiary substrates, a protective layer of PMMA with the thickness around 500 nm was introduced on top of the CNMs, followed by heating at 90 °C for 5 min.

The FEBIP experiments were performed in a commercial UHV instrument (Multiscanlab, Omicron Nanotechnology, Germany) with a base pressure of $p < 2 \times 10^{-10}$ mbar. The $\text{Fe}(\text{CO})_5$ precursor was purchased from ACROS Organics with a purity of 99.5%. The quality of the precursor gas was analyzed with a quadrupole mass spectrometer in a dedicated gas analysis chamber (base pressure $< 2 \times 10^{-9}$ mbar). The precursor gas was dosed through a nozzle with an inner diameter of 3 mm and a distance of ≈ 12 mm to the sample surface. Based on simulations using GIS Simulator (version 1.5),^[33] the local pressure increase on the sample surface was calculated to $\approx 30\times$. For a fixed background pressure of 3.0×10^{-7} mbar this corresponds to a local pressure at the surface of about 9×10^{-6} mbar.^[34] A UHV compatible electron column (Leo Gemini) with a resolution of ≈ 3 nm was used for SEM and FEBIP. Together with a hemispherical electron energy analyzer, also local AES and scanning Auger microscopy were conducted. The AFM experiments were performed with a JPK NanoWizard 4 by using tapping mode.

Supporting Information

Supporting Information is available from the Wiley Online Library or from the author.

Acknowledgements

This project received funding from the European Union's Horizon 2020 research and innovation programme under the Marie Skłodowska-Curie Grant Agreement No. 722149. The Erlangen group acknowledges financial support by the research unit FOR 1878/funCOS.

Open access funding enabled and organized by Projekt DEAL.

Conflict of Interest

The authors declare no conflict of interest.

Keywords

2D materials, carbon nanomembranes, electron beam induced depositions, focused electron beam induced processing, iron nanostructures

Received: June 30, 2020

Revised: August 21, 2020

Published online: October 20, 2020

- [1] a) A. C. Ferrari, F. Bonaccorso, V. Fal'Ko, K. S. Novoselov, S. Roche, P. Bøggild, S. Borini, F. H. Koppens, V. Palermo, N. Pugno, *Nanoscale* **2015**, 7, 4598; b) G. R. Bhimanapati, Z. Lin, V. Meunier, Y. Jung, J. Cha, S. Das, D. Xiao, Y. Son, M. S. Strano, V. R. Cooper, *ACS Nano* **2015**, 9, 11509; c) S. Z. Butler, S. M. Hollen, L. Cao, Y. Cui, J. A. Gupta, H. R. Gutiérrez, T. F. Heinz, S. S. Hong, J. Huang, A. F. Ismach, *ACS Nano* **2013**, 7, 2898.
- [2] F. Koppens, T. Mueller, P. Avouris, A. Ferrari, M. Vitiello, M. Polini, *Nat. Nanotechnol.* **2014**, 9, 780.
- [3] Q. H. Wang, K. Kalantar-Zadeh, A. Kis, J. N. Coleman, M. S. Strano, *Nat. Nanotechnol.* **2012**, 7, 699.
- [4] E. Pomerantseva, Y. Gogotsi, *Nat. Energy* **2017**, 2, 17089.
- [5] R. Kurapati, K. Kostarelos, M. Prato, A. Bianco, *Adv. Mater.* **2016**, 28, 6052.
- [6] W. Geyer, V. Stadler, W. Eck, M. Zharnikov, A. Götzhäuser, M. Grunze, *Appl. Phys. Lett.* **1999**, 75, 2401.
- [7] A. Turchanin, A. Götzhäuser, *Adv. Mater.* **2016**, 28, 6075.
- [8] A. Turchanin, M. El-Desawy, A. Götzhäuser, *Appl. Phys. Lett.* **2007**, 90, 053102.
- [9] X. Zhang, C. Neumann, P. Angelova, A. Beyer, A. Götzhäuser, *Langmuir* **2014**, 30, 8221.
- [10] A. Turchanin, A. Beyer, C. T. Nottbohm, X. Zhang, R. Stosch, A. Sologubenko, J. Mayer, P. Hinze, T. Weimann, A. Götzhäuser, *Adv. Mater.* **2009**, 21, 1233.
- [11] P. Angelova, H. Vieker, N.-E. Weber, D. Matei, O. Reimer, I. Meier, S. Kurasch, J. Biskupek, D. Lorbach, K. Wunderlich, *ACS Nano* **2013**, 7, 6489.
- [12] C. T. Nottbohm, A. Beyer, A. S. Sologubenko, I. Ennen, A. Hütten, H. Rösner, W. Eck, J. Mayer, A. Götzhäuser, *Ultramicroscopy* **2008**, 108, 885.
- [13] a) C. T. Nottbohm, A. Turchanin, A. Beyer, R. Stosch, A. Götzhäuser, *Small* **2011**, 7, 874; b) A. Winter, A. George, C. Neumann, Z. Tang, M. J. Mohn, J. Biskupek, N. Masurkar, A. L. M. Reddy, T. Weimann, U. Hübner, *Carbon* **2018**, 128, 106.
- [14] X. Zhang, E. Marschewski, P. Penner, T. Weimann, P. Hinze, A. Beyer, A. Götzhäuser, *ACS Nano* **2018**, 12, 10301.
- [15] a) Y. Yang, R. Hillmann, Y. Qi, R. Korzetz, N. Biere, D. Emmrich, M. Westphal, B. Büker, A. Hütten, A. Beyer, *Adv. Mater.* **2020**, 32, 1907850; b) Y. Yang, P. Dementyev, N. Biere, D. Emmrich, P. Stohmann, R. Korzetz, X. Zhang, A. Beyer, S. Koch, D. Anselmetti, *ACS Nano* **2018**, 12, 4695.
- [16] A. Beyer, A. Turchanin, C. T. Nottbohm, N. Mellech, M. Schnietz, A. Götzhäuser, *J. Vac. Sci. Technol. B* **2010**, 28, C6D5.
- [17] K. Ekinici, M. Roukes, *Rev. Sci. Instrum.* **2005**, 76, 061101.
- [18] Y. D. Sirmaci, Z. Tang, S. Fasold, C. Neumann, T. Pertsch, A. Turchanin, I. Staude, *ACS Photonics* **2020**, 7, 1060.
- [19] a) W. Van Dorp, C. W. Hagen, *J. Appl. Phys.* **2008**, 104, 081301; b) I. Utke, P. Hoffmann, J. Melngailis, *J. Vac. Sci. Technol. B* **2008**, 26, 1197.

- [20] a) M. M. Shawrav, H. D. Wanzenboeck, D. Belic, M. Gavagnin, O. Bethge, M. Schinnerl, E. Bertagnolli, *Phys. Status Solidi* **2014**, 211, 375; b) V. Gopal, V. R. Radmilovic, C. Daraio, S. Jin, P. Yang, E. A. Stach, *Nano Lett.* **2004**, 4, 2059.
- [21] a) W. F. van Dorp, I. Lazić, A. Beyer, A. Götzhäuser, J. B. Wagner, T. W. Hansen, C. W. Hagen, *Nanotechnology* **2011**, 22, 115303; b) W. Van Dorp, A. Beyer, M. Mainka, A. Götzhäuser, T. W. Hansen, J. B. Wagner, C. Hagen, J. T. M. De Hosson, *Nanotechnology* **2013**, 24, 345301.
- [22] a) A. Beyer, H. Vieker, R. Klett, H. M. zu Theenhausen, P. Angelova, A. Götzhäuser, *Beilstein J. Nanotechnol.* **2015**, 6, 1712; b) M. Schnietz, A. Turchanin, C. T. Nottbohm, A. Beyer, H. H. Solak, P. Hinze, T. Weimann, A. Götzhäuser, *Small* **2009**, 5, 2651.
- [23] M. M. Walz, M. Schirmer, F. Vollnhals, T. Lukaszczuk, H. P. Steinrück, H. Marbach, *Angew. Chem., Int. Ed.* **2010**, 49, 4669.
- [24] a) S. Goler, V. Piazza, S. Roddaro, V. Pellegrini, F. Beltram, P. Pingue, *J. Appl. Phys.* **2011**, 110, 064308; b) C. Thiele, A. Felten, T. J. Echtermeyer, A. C. Ferrari, C. Casiraghi, H. Löhneysen, R. Krupke, *Carbon* **2013**, 64, 84; c) B. Sommer, J. Sonntag, A. Ganczarczyk, D. Braam, G. Prinz, A. Lorke, M. Geller, *Sci. Rep.* **2015**, 5, 7781.
- [25] F. Tu, M. Drost, F. Vollnhals, A. Späth, E. Carrasco, R. Fink, H. Marbach, *Nanotechnology* **2016**, 27, 355302.
- [26] F. Porriati, R. Sachser, M. Walz, F. Vollnhals, H. Steinrück, H. Marbach, M. Huth, *J. Phys. D: Appl. Phys.* **2011**, 44, 425001.
- [27] Z. Liu, A. Cui, J. Li, C. Gu, *Adv. Mater.* **2019**, 31, 1802211.
- [28] F. Tu, *Ph.D. Thesis*, Friedrich-Alexander Universität Erlangen-Nürnberg, **2017**.
- [29] a) F. Vollnhals, P. Wintrich, M.-M. Walz, H.-P. Steinrück, H. Marbach, *Langmuir* **2013**, 29, 12290; b) M. Drost, F. Tu, L. Berger, C. Preischl, W. Zhou, H. Gliemann, C. Wöll, H. Marbach, *ACS Nano* **2018**, 12, 3825.
- [30] M. Schirmer, M.-M. Walz, C. Papp, F. Kronast, A. X. Gray, B. Balke, S. Cramm, C. S. Fadley, H.-P. Steinrück, H. Marbach, *Nanotechnology* **2011**, 22, 475304.
- [31] L. Berger, K. Madajska, I. B. Szymanska, K. Höflich, M. N. Polyakov, J. Jurczyk, C. Guerra-Nunez, I. Utke, *Beilstein J. Nanotechnol.* **2018**, 9, 224.
- [32] M. M. Shawrav, P. Taus, H. D. Wanzenboeck, M. Schinnerl, M. Stöger-Pollach, S. Schwarz, A. Steiger-Thirsfeld, E. Bertagnolli, *Sci. Rep.* **2016**, 6, 34003.
- [33] V. Friedli, I. Utke, *J. Phys. D: Appl. Phys.* **2009**, 42, 125305.
- [34] M. Schirmer, M. Walz, F. Vollnhals, T. Lukaszczuk, A. Sandmann, C. Chen, H. Steinrück, H. Marbach, *Nanotechnology* **2011**, 22, 085301.